Low-velocity impact (LVI) and compression after impact (CAI) of Double-Double composite laminates

Shabani, Peyman; Li, Lucy; Laliberte, Jeremy

Publisher's version / Version de l'éditeur:
https://doi.org/10.1016/j.compstruct.2024.118615
Composite Structures, 351, C, 2024-09-26

Composite Structures 351 (2025) 118615

Contents lists available at ScienceDirect

Composite Structures

journal homepage: www.elsevier.com/locate/compstruct

Low-velocity impact (LVI) and compression after impact (CAI) of Double-Double composite laminates

Peyman Shabani [a,*], Lucy Li [b,*], Jeremy Laliberte [a,*]

[a] Department of Mechanical and Aerospace Engineering, Carleton University, 1125 Colonel By Drive, Ottawa, ON K1S 5B6, Canada
[b] Aerospace Research Centre, National Research Council Canada, 1200 Montreal Road, Ottawa, ON K1A 0R6, Canada

ARTICLE INFO

Keywords:
Composite laminates
Low-velocity impact
Compression after impact
Double-Double laminates

ABSTRACT

Tailorability is a key advantage of fiber-reinforced composites over other material systems. While tailoring a single isolated laminate is relatively simple, challenges arise when designing larger integrated components while ensuring compatibility between laminates and avoiding sharp changes in local stiffness. The innovative Double-Double (DD) laminate design method simplifies the optimization and processing of laminates by incorporating 4-ply building blocks consisting of $+\phi$, $-\phi$, $+\psi$, and $-\psi$ ply orientations. As a relatively new concept, DD laminate design requires careful assessment to ensure its performance is equivalent to that of conventional designs. The current study compares impact damage tolerance of quadriaxial (QUAD) laminates consisting of 0°, 90°, and ±45° ply orientations with equivalent DD laminates under Low-Velocity Impact (LVI) and Compression After Impact (CAI) loadings. To this end, a validated three-dimensional high-fidelity finite element model capable of capturing fiber breakage, splitting, kinking, as well as matrix cracking and delamination, was used. A computer tool was developed to identify equivalent DD laminates and to find the best stacking sequence for achieving layup homogenization. Three equivalent DD laminates were selected for the $[0/45/90/-45]_{4s}$. The first laminate had an equal in-plane stiffness [A] matrix ($[67.5/-22.5/22.5/-67.5]_{8T}$), the second laminate had an equal flexural stiffness [D] matrix ($[64.5/-17/17/-64.5]_{8T}$), and the third laminate ($[65.5/-18.5/18.5/-65.5]_{8T}$) had a similar [D] matrix while keeping the difference between each element of [A] matrices below 10 %. The results indicate that the QUAD laminates can be replaced by equivalent DD without compromising impact damage tolerance while benefiting from the improved design and manufacturing ease of the DD laminate configuration.

1. Introduction

Conventional quadriaxial (QUAD) composite laminates consisting of 0°, ±45°, and 90° plies have been used since the 1960s in advanced composite components. By changing the stacking sequence and the relative percentage of each ply orientation, the laminate can be tailored for a specific loading condition. The tailorability advantage of fiber-reinforced composites is occasionally compromised by design complexity, leading to the adoption of quasi-isotropic layups as a safe and well-understood design choice for many applications, especially those where the composite design is replacing an isotropic metallic design. To ensure manufacturability and damage tolerance, some layup design rules are usually applied such as maintaining mid-plane symmetry to avoid warpage, having at least 10 % of each QUAD angle to withstand unforeseen loads, and ply groups of less than 4 plies of the same angle each to minimize interlaminar stresses. However, even with these layup constraints, the number of QUAD stacking permutations is so high that it makes optimization a difficult task. Double-Double (DD) is an innovative concept introduced by Tsai [1], which incorporates 4-ply building blocks consisting of $+\phi$, $-\phi$, $+\psi$, and $-\psi$ ply orientations. The DD design approach simplifies the design and processing of composite laminates by reducing design complexity from millions of choices to selecting the ϕ and ψ angles and determining the number of building block repetitions.

A limited number of studies have been carried out and published on the DD concept since its introduction in 2017 [2]. The manufacturing opportunities that can be enabled by the DD concept were discussed by Kappel [3]. The feasible design range for the DD layups was obtained by Zhao et al. [4]. The different DD stacking sequences were analyzed by Miravete [5]. Kappel [6] found the best DD stacking sequence and the

* Corresponding authors.
E-mail addresses: peyman.shabani@carleton.ca (P. Shabani), lucy.li@nrc-cnrc.gc.ca (L. Li), jeremy.laliberte@carleton.ca (J. Laliberte).

https://doi.org/10.1016/j.compstruct.2024.118615
Received 9 July 2024; Received in revised form 9 September 2024; Accepted 23 September 2024
Available online 26 September 2024

required number of building block repetitions for panels used in aircraft fuselage and wings based on classical lamination theory (CLT) and mixed integer distributed ant colony optimization (MIDACO) technique. Shrivastava et al. [7] used an artificial intelligence genetic algorithm-based stochastic optimizer to replace QUAD wing-box panels with DD panels and reported a 24 % mass reduction attributed to the absence of mid-plane symmetry requirement in the DD panels. Vermes et al. [8] conducted an analytical study on composite shaft and bulkhead and reported a 6 % weight reduction in both cases by replacing the QUAD with DD. In addition, Vermes et al. [9] conducted fatigue tests on DD laminates with [±0/±25] and [±0/±50] building blocks and observed similar fatigue lives compared to their equivalent QUAD laminates. Alves et al. [10] simulated the damage onset in a composite single lap joint and observed a smoother transition of stress invariants and a 25 % improvement in the damage onset corresponding force for an equivalent DD laminate. The mode-I delamination damage mechanisms of DD laminates were studied by Zhao et al. [11]. Two DD layups with $\psi = 62^\circ$ and $\phi = 9^\circ$, and $\psi = 72^\circ$ and $\phi = 19^\circ$ were investigated and it was observed that the steady-state fracture toughness of laminates at ψ/ϕ interfaces was 20 % higher than that at the $-\psi/\phi$ interfaces. Barbosa et al. [12] compared the performance of hydrogen storage tanks using QUAD and DD laminates in an explosion scenario using an FE model. The equivalent DD laminate exhibited higher stress levels and higher deformation. The notched [13] and open-hole tension [14] responses of DD laminates have also been investigated numerically.

To date, only three publications are available on low-velocity impact (LVI) and compression after impact (CAI) of DD laminates. Cunha et al. [15] conducted LVI and CAI tests on a QUAD $[0_3/90/\pm45/0_2/\pm45]_{2s}$ laminate and its equivalent DD with a similar in-plane stiffness matrix [A] with a stacking sequence of $[\pm0/\pm50]_{10T}$, where "T" denotes total. Both laminates were impacted at a 74 J energy level. The delamination areas were compared through X-ray CT inspections. The difference between the CAI strengths of QUAD and DD (3 %) was within the standard deviation (11.5 %). However, the delamination area in the DD laminate was larger. The lower flexural stiffness of the equivalent DD was mentioned as the reason for this observation. Millen et al. [16] conducted a numerical study on LVI and CAI responses of DD laminates. An equivalent DD to a QUAD with a layup of $[0_2/45_2/90_2/-45_2]_s$ with a similar flexural stiffness matrix [D] was found to be $[9.5/-39.5/39.5/-9.5]_{4T}$. After a 25 J impact event, the CAI strength of the equivalent DD was 40 % higher than that of the QUAD. The 47 % higher stiffness in the loading direction (A_{11} component of [A]) was identified to be the reason for this significant difference. Kappel et al. [17] investigated the CAI of the tapered QUAD and its equivalent DD with a similar [A] matrix after impact on the thickness transition zone. In DD, ply drop-offs were located on the laminate's outer surface. An inferior CAI strength was reported for the DD laminate when impacted on the thickness transition zone.

Based on the published studies, it remains unclear whether replacing a QUAD with an equivalent DD would yield any benefits in terms of impact damage tolerance. The focus of the current study was on the assessment of the performance of the DD laminates under low-velocity impact loading. A validated three-dimensional (3D) high-fidelity finite element (FE) model [18,19] able to capture fiber breakage, splitting, kinking, pull-out, and crushing, as well as matrix cracking and delamination was used to assess the effectiveness of replacing QUAD laminates with equivalent DD laminates under both LVI and CAI loadings. Three equivalent DD laminates for 254 mm × 304.8 mm $[0/45/90/-45]_{4s}$ IM7/977-3 were selected for investigation: 1-with equal [A] matrix, 2-with equal [D] matrix, and 3-with a similar [D] matrix while its [A] matrix overall difference is below 10 %.

2. Equivalent double-double laminate

2.1. Finding equivalent DD laminates

The procedure for finding a DD laminate with a similar [A] or [D] matrix is provided in this section. In orthotropic laminates, the relation between forces (N_i) and moments (M_i) and in-plane strains (ε_i) and curvatures (k_i), where $i = 1, 2, 6$, can be established as Eq. (1):

$$\begin{Bmatrix} N_1 \\ N_2 \\ N_6 \\ M_1 \\ M_2 \\ M_6 \end{Bmatrix} = \begin{bmatrix} A_{11} & A_{12} & A_{16} & B_{11} & B_{12} & B_{16} \\ A_{21} & A_{22} & A_{26} & B_{21} & B_{22} & B_{26} \\ A_{61} & A_{62} & A_{66} & B_{61} & B_{62} & B_{66} \\ B_{11} & B_{12} & B_{16} & D_{11} & D_{12} & D_{16} \\ B_{21} & B_{22} & B_{26} & D_{21} & D_{22} & D_{26} \\ B_{61} & B_{62} & B_{66} & D_{61} & D_{62} & D_{66} \end{bmatrix} \begin{Bmatrix} \varepsilon_1 \\ \varepsilon_2 \\ \varepsilon_6 \\ k_1 \\ k_2 \\ k_6 \end{Bmatrix} \tag{1}$$

where A_{ij}, B_{ij}, and D_{ij} $(i, j = 1, 2, 6)$ are components of the in-plane, coupling, and flexural stiffness matrices of the laminate and have the relation shown in Eq. (2) with the stiffness of a unidirectional ply.

$$\begin{aligned} A_{ij} &= \int_{-h/2}^{h/2} Q_{ij}\, dz \\ B_{ij} &= \int_{-h/2}^{h/2} Q_{ij}\, z\, dz \\ D_{ij} &= \int_{-h/2}^{h/2} Q_{ij}\, z^2\, dz \end{aligned} \tag{2}$$

In Eq. (2), h is the laminate thickness, z indicates the location of the ply with respect to the laminate's mid-plane in the thickness direction, and Q_{ij} $(i,j = 1, 2, 6)$ are the ply stiffness in the global coordinate system. Q_{ij} can be obtained for each ply using Eq. (3) by having its fiber orientation (θ) and in-plane material properties.

$$\begin{aligned} Q_{11} &= U_1 + cos2\theta \times U_2 + cos4\theta \times U_3 \\ Q_{22} &= U_1 - cos2\theta \times U_2 + cos4\theta \times U_3 \\ Q_{12} &= U_4 - cos4\theta \times U_3 \\ Q_{66} &= U_5 - cos4\theta \times U_3 \\ Q_{16} &= \frac{1}{2} sin2\theta \times U_2 + sin4\theta \times U_3 \\ Q_{26} &= \frac{1}{2} sin2\theta \times U_2 - sin4\theta \times U_3 \end{aligned} \tag{3}$$

In Eq. (3), U_i (i = 1,2,3,4,5) are a combination of on-axis ply stiffnesses and they can be obtained as shown in Eq. (4):

$$\begin{aligned} U_1 &= \frac{1}{8}\left[3Q_{xx} + 3Q_{yy} + 2Q_{xy} + 4Q_{ss}\right] \\ U_2 &= \frac{1}{2}\left[Q_{xx} - Q_{yy}\right] \\ U_3 &= \frac{1}{8}\left[Q_{xx} + Q_{yy} - 2Q_{xy} - 4Q_{ss}\right] \\ U_4 &= \frac{1}{8}\left[Q_{xx} + Q_{yy} + 6Q_{xy} - 4Q_{ss}\right] \\ U_5 &= \frac{1}{8}\left[Q_{xx} + Q_{yy} - 2Q_{xy} + 4Q_{ss}\right] \end{aligned} \tag{4}$$

where, Q_{ij} $(i,j{=}x, y, s)$ are on-axis ply stiffnesses and can be found by having the in-plane stiffnesses as shown in Eq. (5):

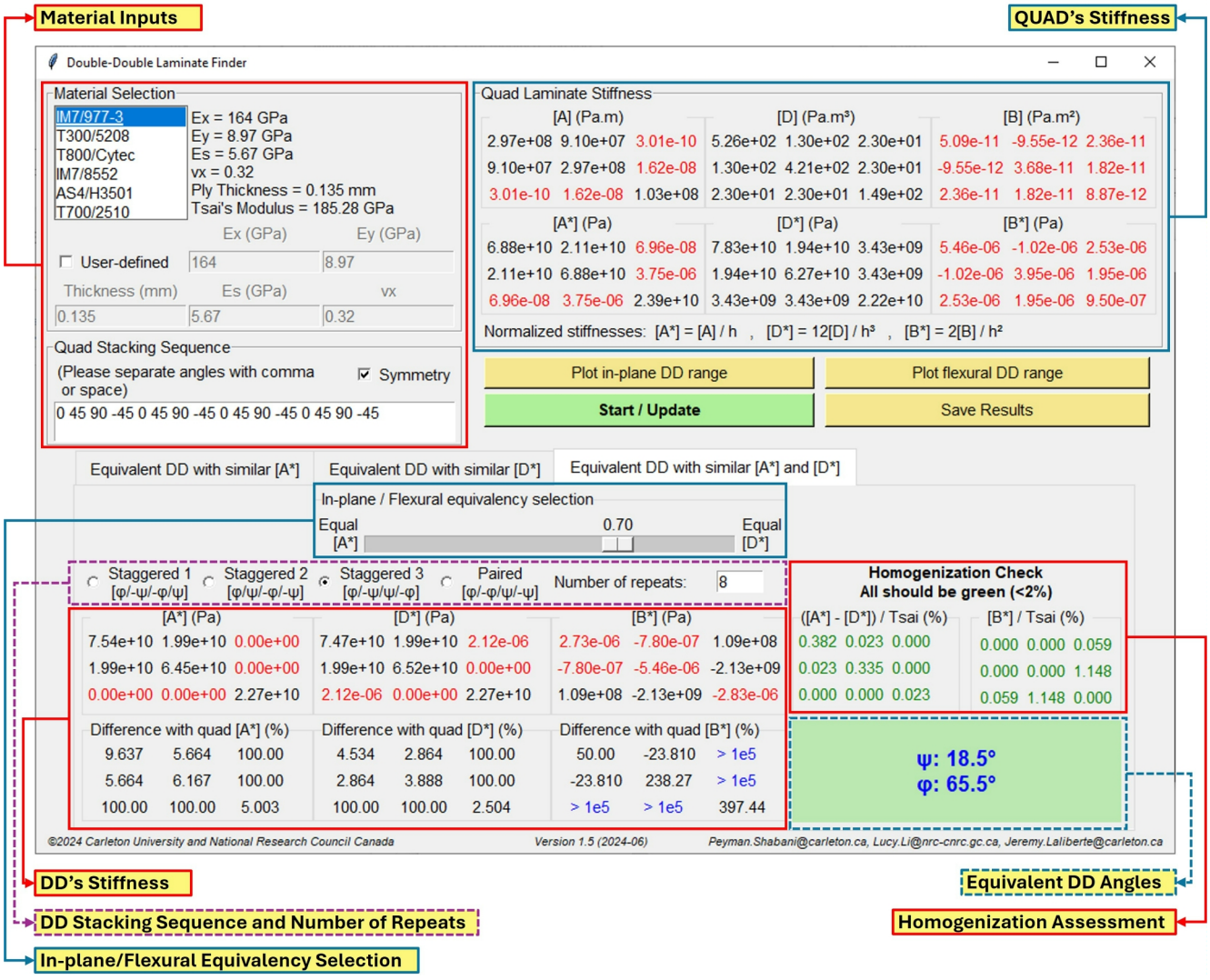

Fig. 1. Developed tool for finding equivalent Double-Double laminates.

$$
\begin{aligned}
Q_{xx} &= mE_x \\
Q_{yy} &= mE_y \\
Q_{xy} &= m\nu_y E_x \\
Q_{yx} &= m\nu_x E_y \\
Q_{ss} &= E_s \\
m &= \frac{1}{1-\nu_x\nu_y}
\end{aligned}
\tag{5}
$$

where, E_x, E_y and E_s are the Young's moduli of the unidirectional ply in the fiber, perpendicular to the fiber and shear directions, respectively; and ν_x and ν_y are the longitudinal and transverse Poisson's ratios.

By substituting Eq. (3) into Eq. (2), and normalizing it with the thickness of the laminate, the components of the normalized laminate in-plane stiffness, A^*_{ij}, can be obtained as shown in Eq. (6). Normalization of the stiffness has two benefits: first, it makes the parameter dimensionless and valid for all systems of units; second, it allows for a direct comparison between the stiffness of the laminate and that of the constituent plies [20].

$$
\begin{aligned}
A^*_{11} &= U_1 + U_2V^*_{A1} + U_3V^*_{A2} \\
A^*_{22} &= U_1 - U_2V^*_{A1} + U_3V^*_{A2} \\
A^*_{12} &= U_4 - U_3V^*_{A2} \\
A^*_{66} &= U_5 - U_3V^*_{A2} \\
A^*_{16} &= \frac{1}{2}U_2V^*_{A3} + U_3V^*_{A4} \\
A^*_{26} &= \frac{1}{2}U_2V^*_{A3} - U_3V^*_{A4}
\end{aligned}
\tag{6}
$$

In Eq. (6), V^*_{Ai} ($i = 1,2,3,4$) are normalized geometric factors for the in-plane stiffness and are related to the fiber orientations of the laminate's constituent plies and can be obtained by using Eq. (7).

$$V_{A1}^{*}=\frac{1}{h}\int_{-\frac{h}{2}}^{\frac{h}{2}}\cos2\theta dz$$
$$V_{A2}^{*}=\frac{1}{h}\int_{-\frac{h}{2}}^{\frac{h}{2}}\cos4\theta dz$$
$$V_{A3}^{*}=\frac{1}{h}\int_{-\frac{h}{2}}^{\frac{h}{2}}\sin2\theta dz \quad (7)$$
$$V_{A4}^{*}=\frac{1}{h}\int_{-\frac{h}{2}}^{\frac{h}{2}}\sin4\theta dz$$

Considering Eq. (6), it can be observed that the normalized in-plane stiffness matrix [A*] is related to the material properties through U_i and to the ply orientations through V_{Ai}^{*}. Hence, for a DD laminate, made of the same material, to have a similar [A*], the V_{Ai}^{*} should be equal to those of the QUAD laminate. For a DD laminate, the normalized geometric factors for the in-plane stiffness (V_{Ai}) can be found as shown in Eq. (8):

$$V_{A1}^{*}=\frac{1}{2}(\cos2\phi+\cos2\psi)$$
$$V_{A2}^{*}=\frac{1}{2}(\cos4\phi+\cos4\psi) \quad (8)$$
$$V_{A3}^{*}=V_{A4}^{*}=0$$

where ϕ and ψ are the fiber orientations of the DD laminate. Rearrangement of Eq. (8) gives Eq. (9):

$$\cos2\phi=2V_{A1}^{*}-\cos2\psi$$
$$\cos^{2}2\psi=V_{A2}^{*}-\cos^{2}2\phi+1 \quad (9)$$

which can be used to determine the ϕ and ψ angles. To this end, the first line of Eq. (9) can be substituted into the second line of Eq. (9), which gives Eq. (10). Subsequently, Eq. (10) can be substituted into the first line of Eq. (9) to find the ϕ angle.

$$\cos2\psi=V_{A1}^{*}+\sqrt{-{V_{A1}^{*}}^{2}+\frac{V_{A2}^{*}}{2}+\frac{1}{2}} \quad (10)$$

The procedure of finding an equivalent DD laminate with a similar [D*] matrix is similar to what was mentioned for a DD laminate with a similar [A*]. For a DD laminate to have a similar [D*] matrix to a QUAD laminate, its normalized geometric factors for the flexural stiffness, V_{Di}^{*} (i = 1,2,3,4), should be similar to those of the QUAD laminate. The normalized geometric factors for the flexural stiffness are shown in Eq. (11).

$$V_{D1}^{*}=\frac{12}{h^{3}}\int_{-\frac{h}{2}}^{\frac{h}{2}}\cos2\theta z^{2}dz$$
$$V_{D2}^{*}=\frac{12}{h^{3}}\int_{-\frac{h}{2}}^{\frac{h}{2}}\cos4\theta z^{2}dz \quad (11)$$
$$V_{D3}^{*}=V_{D4}^{*}=0$$

The ϕ and ψ angles of the equivalent DD laminate with a similar V_{Di} can be obtained using Eq. (12).

$$\cos2\psi=V_{D1}^{*}+\sqrt{-{V_{D1}^{*}}^{2}+\frac{V_{D2}^{*}}{2}+\frac{1}{2}} \quad (12)$$
$$\cos2\phi=2V_{D1}^{*}-\cos2\psi$$

2.2. DD laminate finder computer tool

A computer tool with a graphical user interface, shown in Fig. 1, was developed to determine the DD laminate with an equivalent in-plane stiffness [A] or flexural stiffness [D], evaluate the material homogenization conditions, and find the best DD stacking sequence in terms of homogenization based on classical lamination theory (CLT). The source code of this tool is provided in the supplementary material.

In the "Material Inputs" section, the material properties and the stacking sequence of the QUAD laminate can be entered. In the "In-plane/Flexural Equivalency Selection" section, the equivalency of DD's [A*] and [D*] to QUAD can be selected. If the in-plane/flexural equivalency of 0 and 1 is chosen, the ψ angle would be found from Eqs. (10) and (12), respectively. In the case of choosing another value, the ψ angle would be found through interpolation. In the "DD Stacking Sequence and Number of Repeats" section, the stacking sequence of the DD building block and the number of building block repeats can be specified. In the "QUAD's Stiffness" section, the [A], [B] and [D] matrices and their normalized values are calculated. In the "DD's stiffness" section, normalized [A*], [B*] and [D*] matrices are provided, along with their differences from QUAD's normalized stiffness. The homogenization condition would also be evaluated for the equivalent DD angles, the specified stacking sequence and the number of building block repeats in the "Homogenization Assessment" section. This tool can also plot the in-plane and flexural DD design ranges and indicate if the QUAD is outside the DD design range. This will be discussed in more detail in the following sections.

For comparing the stiffnesses of the DD and QUAD laminates, the stiffness matrices were normalized by the laminate thickness:

$$[A^{*}]=\frac{1}{h}[A],[B^{*}]=\frac{2}{h^{2}}[B],[D^{*}]=\frac{12}{h^{3}}[D] \quad (13)$$

The equivalent DD laminate with an equal normalized in-plane stiffness [A*], has the same A_{11}^{*}, A_{22}^{*}, A_{66}^{*}, and A_{12}^{*}, and the equivalent DD laminate with an equal normalized flexural-plane stiffness [D*], has the same D_{11}^{*}, D_{22}^{*}, D_{66}^{*}, and D_{12}^{*}, where A_{ij}^{*} and D_{ij}^{*} (i, j=1,2,6) are components of the normalized in-plane and flexural stiffness matrices. Depending on whether the in-plane stresses or the bending stresses dominate in the desired application, an equivalent DD with equal [A*] or [D*] could be found. In the case of LVI, since the bending stiffness plays the main role in the impact response of the laminate, an equivalent DD with similar [D*] will exhibit a similar response to the original QUAD laminate. Conversely, in the compression test, the in-plane stiffness [A*], specifically A_{11}^{*}, is more important in determining the effective compressive modulus of the laminate. In the current study, since both impact damage and CAI strength were of interest, a DD laminate was chosen with a similar [D*] matrix while keeping the difference between each element of [A*] matrices of DD and QUAD below 10 %. In this way, the DD laminate would have similar (but not equal) in-plane and flexural stiffnesses to those of the QUAD laminate.

The DD characteristics come from their homogenized properties. When a laminate is homogenized, its properties are uniform across the thickness direction. Homogenization is a key feature of DD laminates that allows for the addition and removal of 4-ply building blocks without altering the laminate's normalized stiffness and without the need to worry about violating stacking sequence symmetry. This feature enables several manufacturing advantages, such as tapering, which can save weight and result in highly optimized parts.

A laminate is homogenized when its normalized in-plane stiffness [A*] is equal to its normalized flexural stiffness [D*], and its coupling matrix is zero ([B*] = 0) [1,6]. The former homogenization criterion comes from Eq. (2). In a homogenized material, Q_{ij} is constant throughout the thickness. Therefore, the normalized in-plane and flexural stiffnesses are equal. The latter homogenization criterion is associated with the warpage after the curing process. In homogenized materials and heterogeneous laminates with a symmetric layup, the normalized coupling matrix [B*] is zero. In practice, since the DD laminate is not symmetric, it is not possible for [B*] to become zero.

Table 1
Stacking sequences of equivalent DD laminates.

ID	Stacking Sequence	Feature
QUAD	$[0/45/90/-45]_{4S}$	Baseline configuration
DD1	$[67.5/-22.5/22.5/-67.5]_{8T}$	Equal [A*]
DD2	$[64.5/-17/17/-64.5]_{8T}$	Equal [D*]
DD3	$[65.5/-18.5/18.5/-65.5]_{8T}$	Difference in [A*] < 10 %, Difference in [D*] < 5 %

Therefore, the following criteria have been suggested for checking the homogenization condition [1,6]. These criteria ensure a uniform stress distribution along the thickness and minimize warpage.

$$[A^*] - [D^*] < 0.02 \times \textit{Tsai's modulus} \tag{14}$$

$$[B^*] < 0.02 \times \textit{Tsai's modulus} \tag{15}$$

where the Tsai's modulus is:

$$\textit{Tsai's modulus} = A^*_{11} + A^*_{22} + 2 \times A^*_{66} \tag{16}$$

There are four types of DD laminates referred to as "staggered 1" ($[+\phi/-\psi/-\phi/+\psi]$), "staggered 2" ($[+\phi/+\psi/-\phi/-\psi]$), "staggered 3" ($[+\phi/-\psi/+\psi/-\phi]$), and "paired" ($[\pm\phi/\pm\psi]$). As the number of building block repeats increases, the laminate converges to the homogenization condition. Depending on the ϕ and ψ angles, one of these stacking sequences becomes homogenized faster than the others and requires a smaller number of repetitions of its building blocks to meet homogenization criteria. The developed tool, "Double-Double Laminate Finder", was utilized for both finding the equivalent DD angles and selecting the best stacking sequence by checking the number of repetitions required to reach homogenization. Three equivalent DD laminates were selected. The stacking sequences and features of these laminates are shown in Table 1. For the selected DD laminates, "staggered 1", "staggered 2", and "staggered 3" reached homogenization after 5 repetitions, and "paired" configuration homogenized after 9 repetitions. Among staggered configurations, "staggered 3" was chosen because it was anti-symmetric, and its stiffness components A^*_{16}, A^*_{26}, D^*_{16}, D^*_{26}, B^*_{11}, B^*_{12}, B^*_{22}, and B^*_{66} were zero.

The normalized [A*], [B*] and [D*] matrices for the QUAD and its equivalent DD laminates are provided in Table 2. Comparing DD1 with QUAD, their [A*] matrices were equal. The D^*_{11} component of DD1 was 13 % lower, and its D^*_{11}, D^*_{12} and D^*_{22} components were less than 10 % higher. Comparing DD2 with QUAD, D^*_{13} and D^*_{23} were zero in DD2, and the other components of their [D*] matrices differed by less than 1 %. The A^*_{11} component of DD2 was 14 % higher, and its A^*_{11}, A^*_{12} and A^*_{22} were less than 9 % lower. Comparing DD3 with QUAD, A^*_{13} and A^*_{23} were zero in DD3, and the other components had less than 10 % difference. Regarding its [D*] matrix, the D^*_{13} and D^*_{23} components were zero in DD3, and the other components had less than 5 % difference. In all DD laminates, unlike in QUAD, the B^*_{13} and B^*_{23} components were not zero. However, they were below 1 % of Tsai's modulus.

3. High-fidelity modeling of LVI and CAI tests

3.1. Finite element model

To predict the LVI damage, a 3D FE model of a 254 mm × 304.8 mm × 4.35 mm (10 in × 12 in × 0.17 in) composite laminate was modeled in Abaqus as illustrated in Fig. 2(a). The base plate and the impactor were modeled as rigid bodies. Contact interactions were established between the edges of the laminate and the three guiding pins of the base plate, between the lower surface of the laminate and the rounded frame of the base plate, and also between the top surface of the laminate and the four rubber clamps. The normal behavior of all contacts was set to "Hard", and the tangential behavior was set to "Penalty" friction formulation with a frictional coefficient of 0.8 between the laminate and the clamps,

Table 2
Normalized stiffnesses of QUAD, DD1, DD2 and DD3 laminates (in GPa).

QUAD: $[0/45/90/-45]_{4S}$

$$[A^*] = \begin{bmatrix} 68.80 & 21.10 & 0.00 \\ 21.10 & 68.80 & 0.00 \\ 0.00 & 0.00 & 23.90 \end{bmatrix} \quad [B^*] = \begin{bmatrix} 0.00 & 0.00 & 0.00 \\ 0.00 & 0.00 & 0.00 \\ 0.00 & 0.00 & 0.00 \end{bmatrix} \quad [D^*] = \begin{bmatrix} 78.30 & 19.40 & 3.43 \\ 19.40 & 62.70 & 3.43 \\ 3.43 & 3.43 & 22.20 \end{bmatrix}$$

DD1: $[67.5/-22.5/22.5/-67.5]_{8T}$

$$[A^*] = \begin{bmatrix} 68.80 & 21.10 & 0.00 \\ 21.10 & 68.80 & 0.00 \\ 0.00 & 0.00 & 23.90 \end{bmatrix} \quad [B^*] = \begin{bmatrix} 0.00 & 0.00 & 0.28 \\ 0.00 & 0.00 & -2.00 \\ 0.28 & -2.00 & 0.00 \end{bmatrix} \quad [D^*] = \begin{bmatrix} 68.10 & 21.10 & 0.00 \\ 21.10 & 69.40 & 0.00 \\ 0.00 & 0.00 & 23.90 \end{bmatrix}$$

DD2: $[64.5/-17/17/-64.5]_{8T}$

$$[A^*] = \begin{bmatrix} 78.30 & 19.40 & 0.00 \\ 19.40 & 62.70 & 0.00 \\ 0.00 & 0.00 & 22.20 \end{bmatrix} \quad [B^*] = \begin{bmatrix} 0.00 & 0.00 & 0.02 \\ 0.00 & 0.00 & -2.17 \\ 0.02 & -2.17 & 0.00 \end{bmatrix} \quad [D^*] = \begin{bmatrix} 77.50 & 19.40 & 0.00 \\ 19.40 & 63.30 & 0.00 \\ 0.00 & 0.00 & 22.20 \end{bmatrix}$$

DD3: $[65.5/-18.5/18.5/-65.5]_{8T}$

$$[A^*] = \begin{bmatrix} 75.40 & 19.90 & 0.00 \\ 19.90 & 64.50 & 0.00 \\ 0.00 & 0.00 & 22.70 \end{bmatrix} \quad [B^*] = \begin{bmatrix} 0.00 & 0.00 & 0.11 \\ 0.00 & 0.00 & -2.13 \\ 0.11 & -2.13 & 0.00 \end{bmatrix} \quad [D^*] = \begin{bmatrix} 74.70 & 19.90 & 0.00 \\ 19.90 & 65.20 & 0.00 \\ 0.00 & 0.00 & 22.70 \end{bmatrix}$$

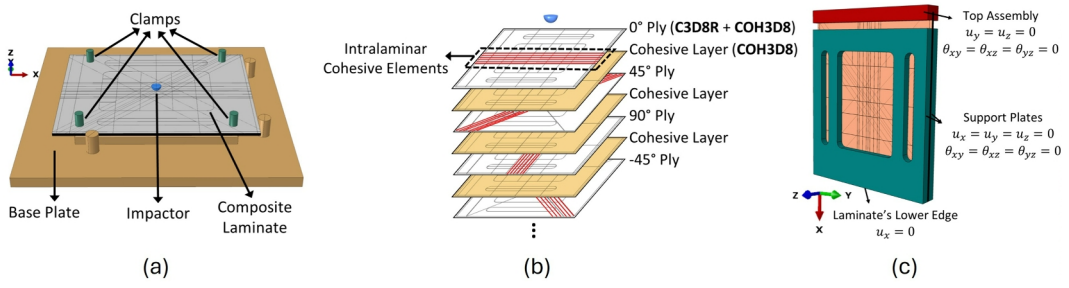

Fig. 2. (a) FE model assembly for LVI simulation, (b) Embedded cohesive elements inside laminate, (c) FE model assembly and boundary conditions for CAI simulation [19].

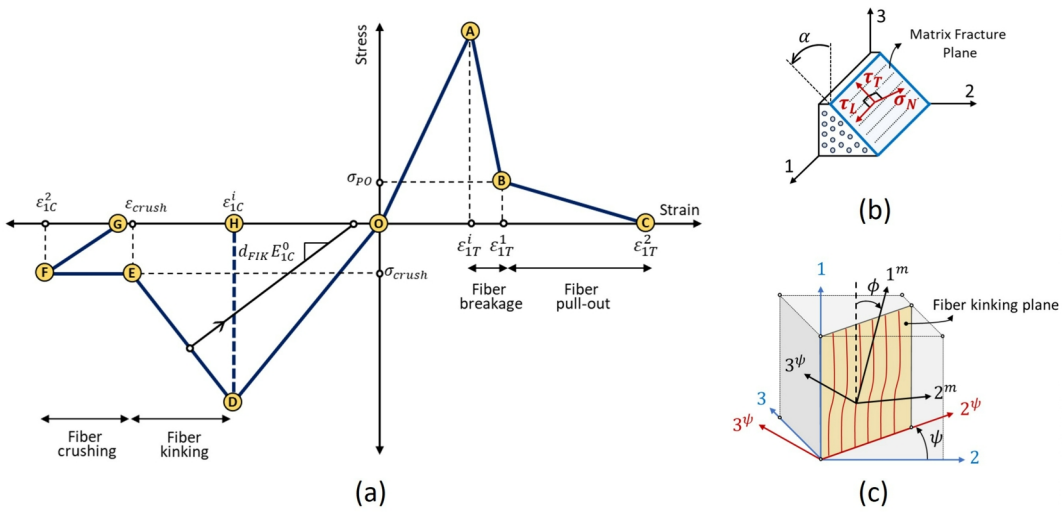

Fig. 3. (a) Fiber damage evolution under tension and compression, (b) matrix fracture plane, (c) fiber kinking plane.

Table 3
Mechanical properties of IM7/977-3 used in the FE model.

Property	Value	Reference
Density, ρ (kg/m^3)	1596	[18]
Tensile longitudinal modulus, E^0_{1T} (GPa)	164	[37]
Compressive longitudinal modulus, E^0_{1C} (GPa)	119	[38]
Transverse modulus, E_2 (GPa)	8.98	[37]
Out-of-plane modulus, E_3 (GPa)	8.88	[18]
In-plane shear modulus, G_{12} (GPa)	5.67	[18]
Out-of-plane shear modulus, G_{13} (GPa)	5.21	[18]
Out-of-plane shear modulus, G_{23} (GPa)	3.14	[18]
In-plane Poisson's ratio, ν_{12}	0.320	[18]
Out-of-plane Poisson's ratio, ν_{13}	0.329	[18]
Out-of-plane Poisson's ratio, ν_{23}	0.461	[18]
Longitudinal tensile strength, X_T (MPa)	2905	[37]
Longitudinal compressive strength, X_C (MPa)	1569	[37]
Transverse tensile strength, Y_T (MPa)	78.9	[37]
Transverse compressive strength, Y_C (MPa)	248	[37]
In-plane shear strength, S_L (MPa)	117.9	[18]
Out-of-plane shear strength, S_T (MPa)	104.7	[18]
Pull-out stress, σ_{PO} (MPa)	173	[39]
Fiber pull-out strain, ε^1_{1T}	0.018	[40]
Fiber crushing stress, σ_{crush} (MPa)	270	[41]
Fiber fracture toughness in tension, G_{1T} (N/mm)	94.1	[42]
Fiber fracture toughness in compression, G_{1C} (N/mm)	47.5	[42]
Ply thickness, t (mm)	0.136	[18]

Table 4
Interface properties of IM7/977-3 [18].

Property	Value
Density, ρ (kg/m^3)	1320
Penalty stiffness, K^0 (N/mm^3)	2×10^5
Mode-I maximum traction, T_n (MPa)	77.2
Mode-II maximum traction, T_s (MPa)	60.0
Mode-III maximum traction, T_t (MPa)	60.0
Mode-I fracture toughness, G_{IC} (N/mm)	0.216
Mode-II fracture toughness, G_{IIC} (N/mm)	0.607
Mode-III fracture toughness, G_{IIIC} (N/mm)	1.272
Mixed-mode power-law exponent, β	2.284

and 0.2 for other contacts. Two impact scenarios were simulated: the first with a hemispherical impactor with a diameter of 25.4 mm, a mass of 6.25 kg and an impact energy of 75 J, and the second with a diameter of 15.8 mm, a mass of 6.14 kg and an impact energy of 30 J. Delamination was captured by embedded 3D cohesive elements (COH3D8) with a thickness of 0.005 mm between the adjacent composite piles. To capture the interaction between intralaminar matrix cracking and delamination [21,22], six rows of 3D cohesive elements with a thickness of 0.02 mm aligned with the fiber directions were deployed in each composite ply, as shown in Fig. 2(b). It should be noted that the modeling was done in the mesoscale. However, the model could capture various fiber failure modes, matrix cracking, delamination and delamination migration from one interface to another.

The ASTM D7137 [23] CAI coupon size is 150 mm × 100 mm. However, this test was designed to assess the residual compressive strength of the composite laminates with barely visible impact damage (BVID). It has been observed that at higher impact energies, the standard laminate becomes fully delaminated [24]. In addition, it has been reported that this relatively small coupon does not accurately represent the residual compressive load-carrying capacity of larger composite panels [25]. Thus, a 254 mm × 304.8 mm laminate with anti-buckling support plates was considered for investigating the LVI and CAI of DD laminates. The effect of using the support plates has been reported in [19].

After the LVI simulation, the predicted impact damage state was transferred to the CAI model using a Python script [19]. The CAI FE model assembly is shown in Fig. 2(c). In the CAI model, the top assembly was allowed to move only in the X-direction to apply the vertical compressive force, and the movement of the laminate's lower edge was constrained in the X-direction. Both the top assembly and the anti-buckling support plates were modeled as rigid bodies. The Abaqus/Explicit was used for the analysis. To reduce the running time of the CAI simulation, mass scaling was used. Abaqus can apply mass scaling either by multiplying the mass of all finite elements by a factor or by defining a target minimum stable time increment (STI) and allowing the FE solver to multiply the mass of each finite element by different factors to achieve this STI. For this simulation, the latter method was used to be able to estimate the simulation time. The target minimum STI of 5×10^{-7} s was used. The STI before mass scaling was 5×10^{-9} s. High mass scaling can increase the inertia and cause errors [26–28]. The target minimum STI was selected to be low enough to minimize oscillations in the force–displacement diagram obtained from the CAI simulation and to ensure that the kinetic energy remains below 5 % of the internal energy. To further reduce the running time, the displacement rate of the top

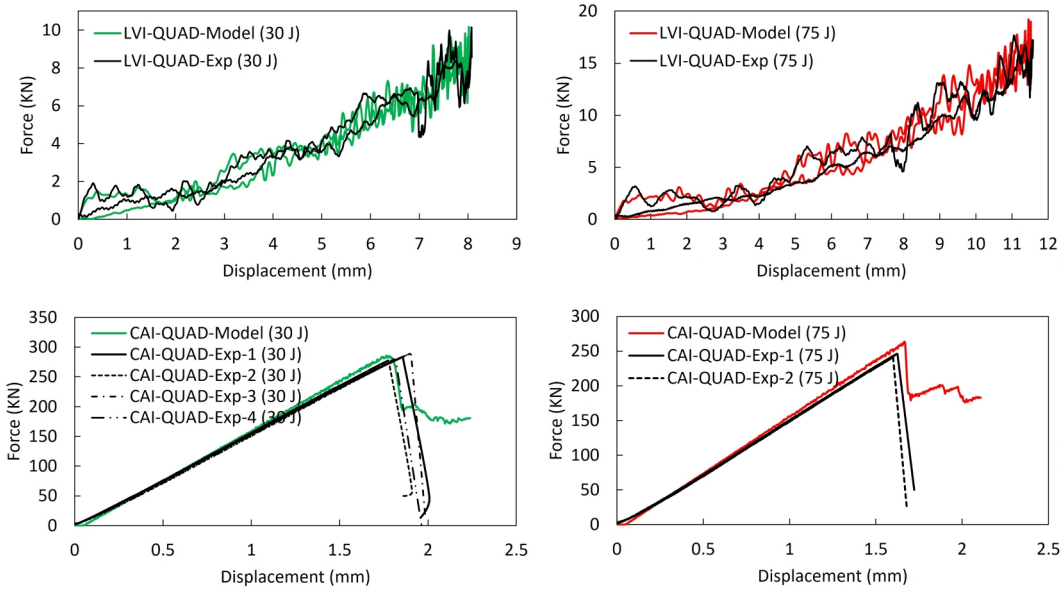

Fig. 4. Predicted and experimental LVI and CAI force–displacement diagrams for the QUAD $[0/45/90/-45]_{4s}$ laminate.

Table 5
Key parameters of LVI responses of QUAD and DD laminates.

75 J Impact				
	QUAD	DD1	DD2	DD3
Impact peak load (kN)	19.1	19.5 (+2.1 %)	18.8 (−1.5 %)	20.4 (+6.8 %)
Impact maximum displacement (mm)	11.5	11.6 (+0.9 %)	11.6 (+0.9 %)	11.6 (+0.9 %)
Impact duration (ms)	7.17	7.19 (+0.3 %)	7.19 (+0.3 %)	7.21 (+0.5 %)
30 J Impact				
	QUAD	DD1	DD2	DD3
Impact peak load (kN)	10.2	10.8 (+5.9 %)	10.6(+3.9 %)	10.7 (+4.9 %)
Impact maximum displacement (mm)	8.0	8.1 (+1.3 %)	8.1 (+1.3 %)	8.1 (+1.3 %)
Impact duration (ms)	7.98	8.07 (+1.1 %)	8.07 (+1.1 %)	8.09 (+1.4 %)

assembly, through which the compressive load was applied, was increased to 5 mm/s, which was 300 times higher than the testing displacement rate of 1 mm/min. Consequently, the CAI simulation was completed in 48 h on a high-performance computer (HPC) with a 2x Intel E5-2683 v4 Broadwell @ 2.1 GHz CPU, which had 16 cores and 32 threads.

3.2. Composite damage modeling methodology

The model captured fiber breakage, splitting, kinking, pull-out, crushing, and matrix cracking using a VUMAT user-defined material subroutine. The physically-based LaRC05 failure criteria performed very well in the World-Wide Failure Exercise II [29]. Additionally, it can distinguish between different composite failure modes. Hence, in this study, for matrix and fiber damage initiation, the enhanced LaRC05 failure criteria [19,30,31] were employed. To predict the fiber damage evolution, a new model was introduced based on the models of Martín-Santos et al. [32] and Rivallant et al. [33]. These two models were modified to be compatible with the LaRC05 criteria [34]. The modeled fiber failure behavior is illustrated in Fig. 3(a).

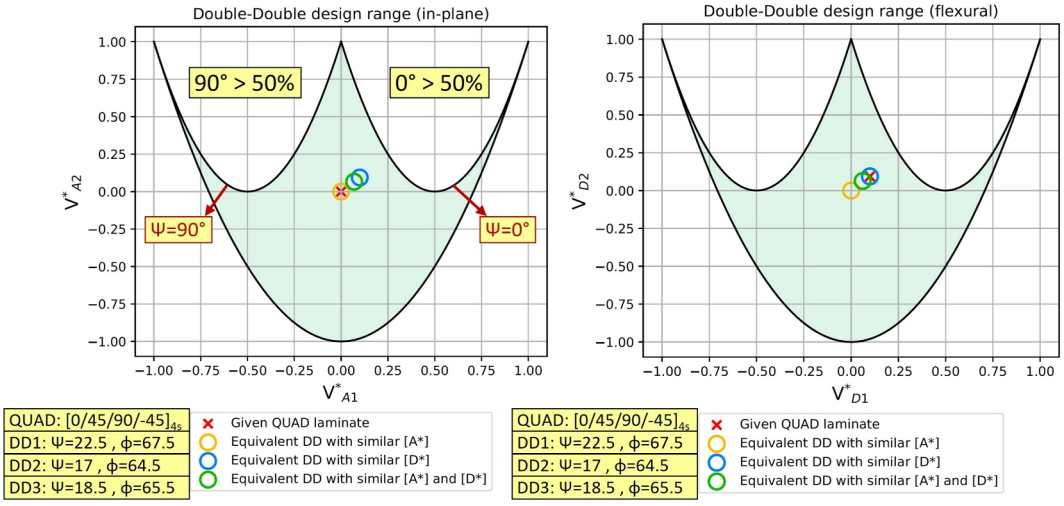

Fig. 5. Design range of DD laminates and the locations of the QUAD, DD1, DD2, and DD3 laminates in the in-plane and flexural design ranges.

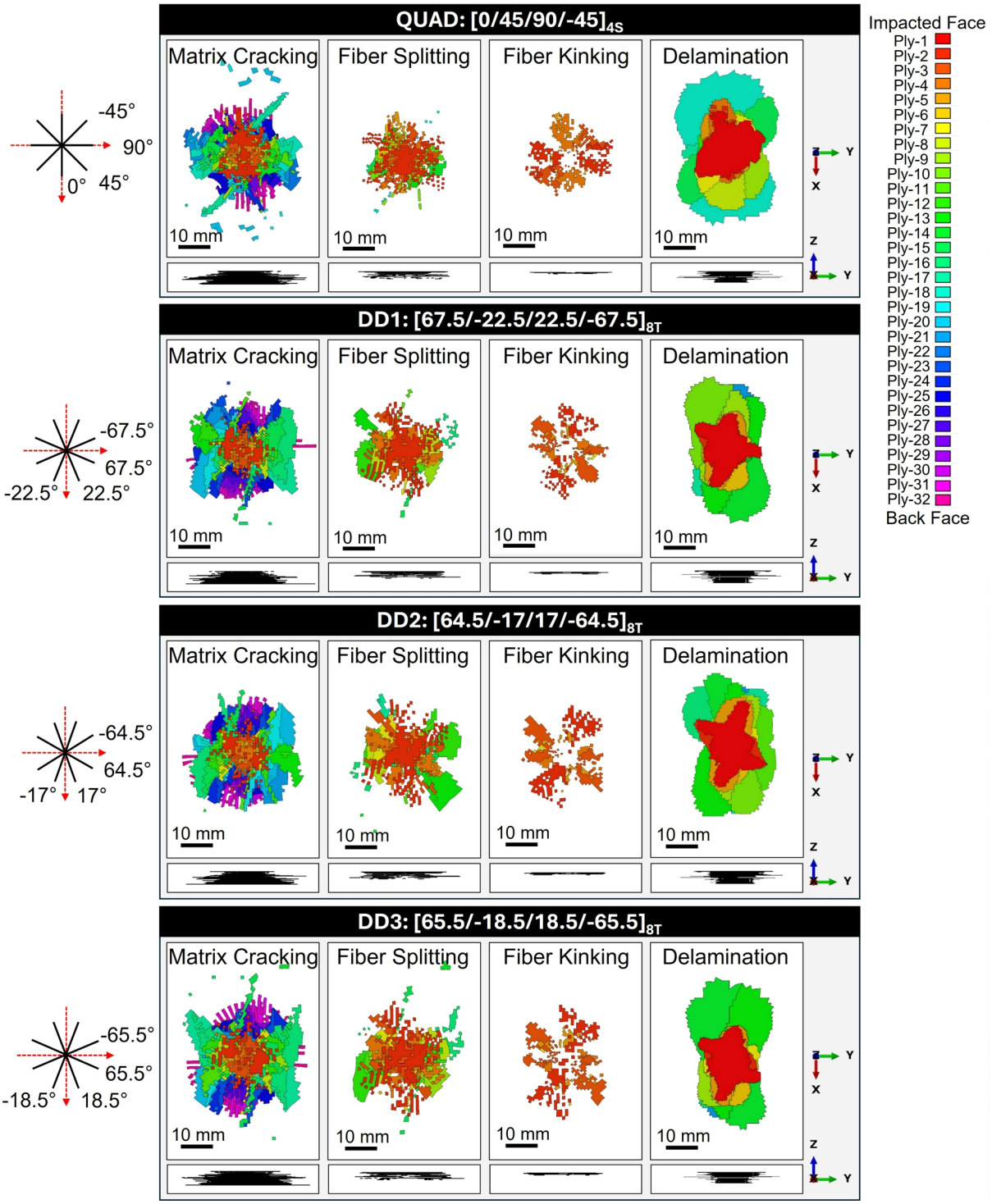

Fig. 6. Inter- and intra-laminar failure modes predicted for the QUAD and the DD laminates after a 75 J impact event.

After the prediction of fiber breakage initiation using the LaRC05 failure criterion (Point A in Fig. 3(a)), the tensile modulus in the fiber direction (E^0_{1T}) underwent a two-stage reduction. First, a sharp decrease happened in E^0_{1T} (Points A to B in Fig. 3(a)) attributed to the processes occurring in the vicinity of the crack tip [32]. This decline in the stiffness continued until the stress in the fiber direction reached the fiber pull-out stress (σ_{PO}). The second stage (Points B to C in Fig. 3(a)) was considered to simulate the energy release caused by the fiber pull-out mechanism. For fiber failure behavior in compression, two forms of damage evolution were considered, depending on whether the damage mode is fiber splitting or fiber kinking. If fiber splitting occurs, Point D in Fig. 3(a), the compressive modulus of the element in the fiber direction would drop to zero (Point H in Fig. 3(a)). However, if fiber kinking occurs, the compressive modulus would decrease until the stress in the fiber direction reaches the fiber crushing stress (σ_{crush}), as Point E shown in Fig. 3(a). After this point, by increasing the compressive load, the two sides of the crack come into contact and result in the crushing of packs of fibers. In the current model, fiber crushing was modeled with a plastic law [35].

In the LaRC05 failure criteria, it is required to find the matrix frac-

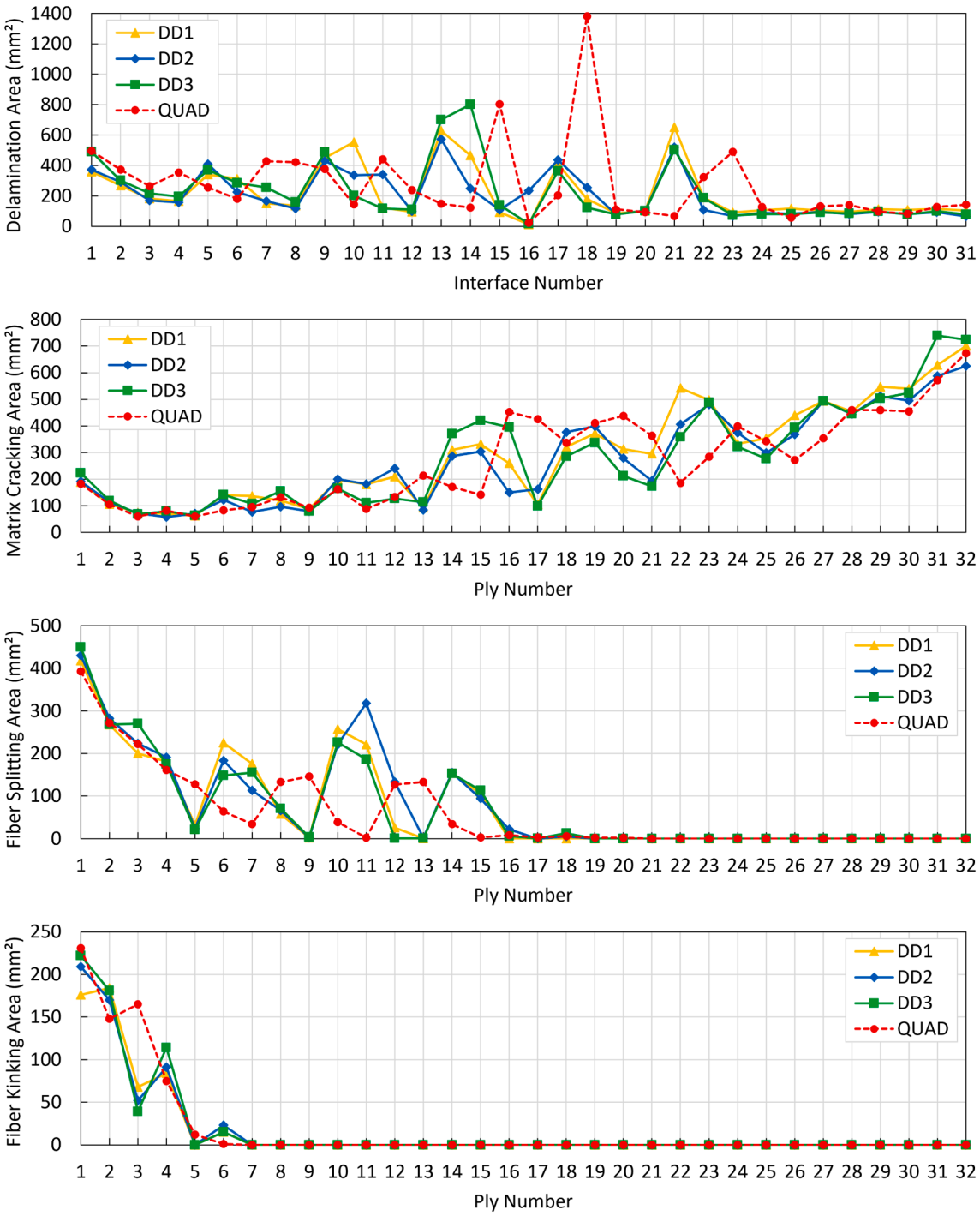

Fig. 7. Ply-by-ply inter- and intra-laminar damage areas in the QUAD and DD laminates after a 75 J impact event. (Ply-1 is near the impacted face.).

ture plane (α) and the fiber kink band angle (ψ) (Fig. 3(b) and (c)). To efficiently determine these angles, the selective range golden section search (SRGSS) algorithm [30,31,36] was employed along with the LaRC05 criteria.

The mechanical properties of IM7/977-3 are shown in Table 3, and the cohesive zone modeling (CZM) parameters are provided in Table 4. The damage modeling methodology used in this study is explained in more detail and validated with experimental results in [18,19]. The experiments were conducted on IM7/977-3 $[0/45/90/-45]_{4s}$ quasi-isotropic laminates under 30 J and 75 J impact scenarios. The 30 J impact tests were conducted with a hemispherical impactor with a 15.87 mm diameter and a mass of 6.14 kg, and the 75 J impact tests were conducted using a hemispherical impactor with a 25.4 mm diameter and a mass of 6.25 kg. The predicted and the experimental LVI and CAI force–displacement diagrams are shown in Fig. 4. Using this modeling methodology for simulating the LVI, the maximum deflection and the contact durations were predicted with less than 2 % error, and the peak force and superimposed damage areas were predicted with less than 8 % error. The residual compressive strength after 30 J and 75 J impact events was predicted with 2 % and 9 % errors, respectively (see Table 5).

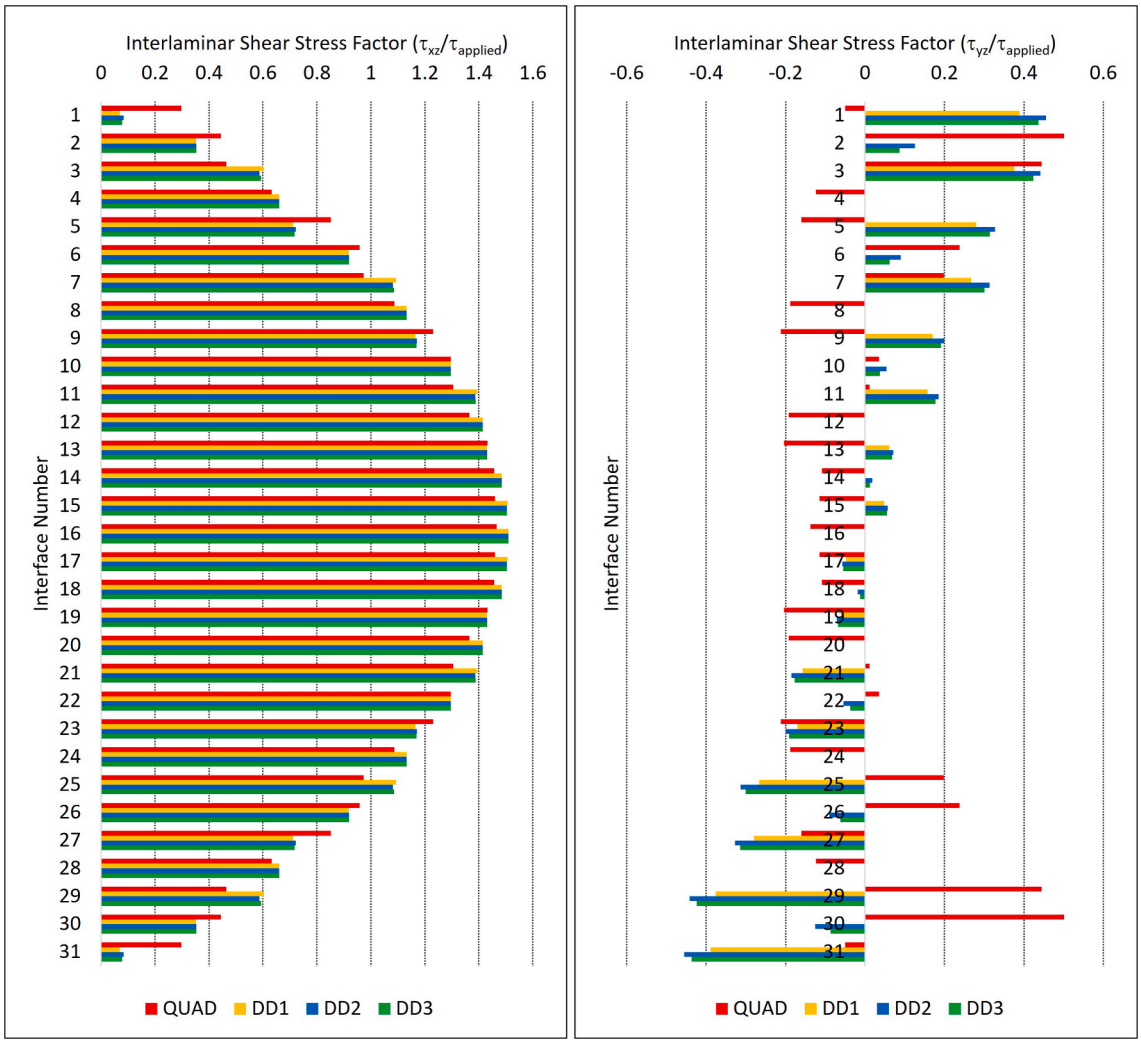

Fig. 8. Layer-by-layer interlaminar shear stress factors in QUAD and DD laminates.

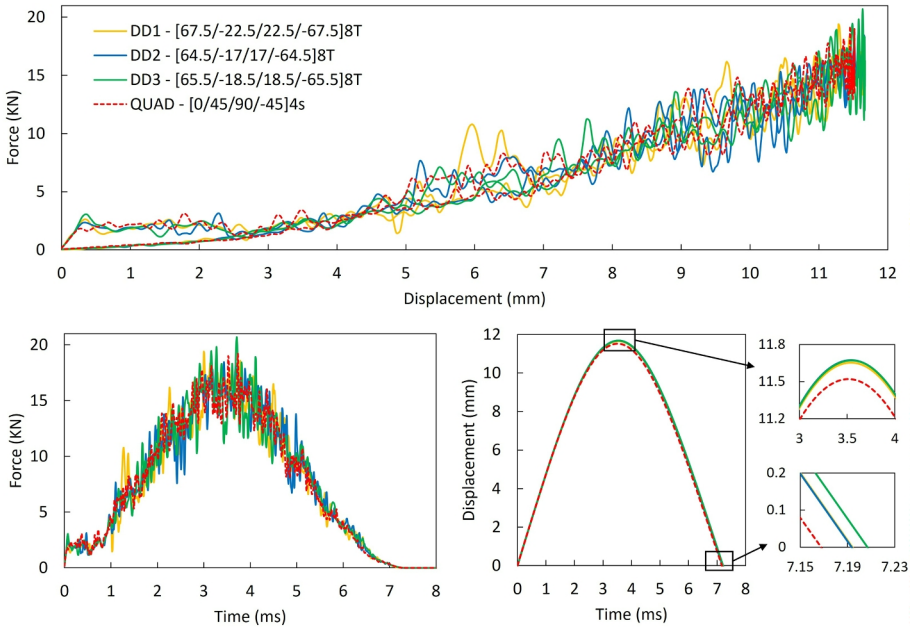

Fig. 9. Responses of QUAD and DD laminates during 75 J LVI event.

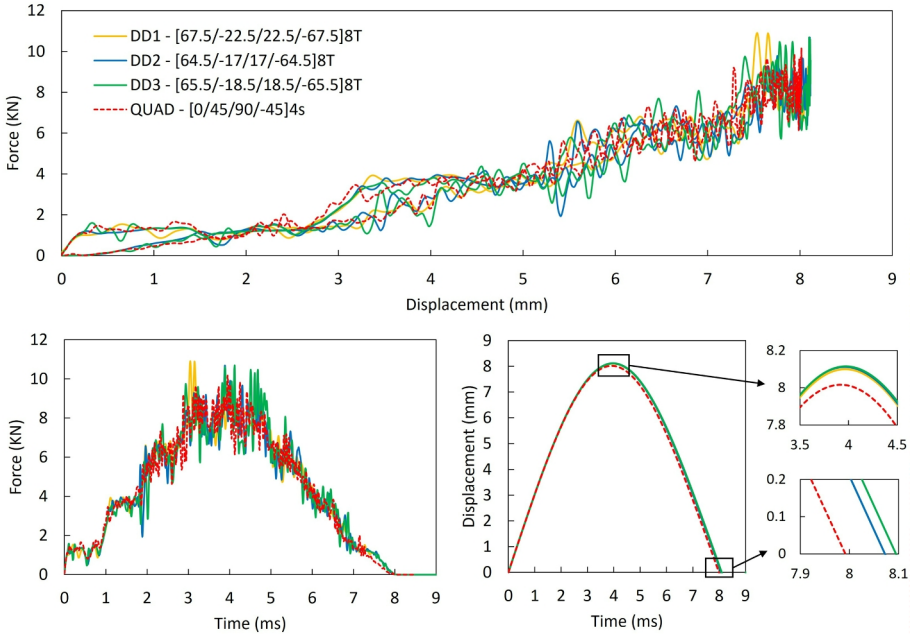

Fig. 10. Responses of QUAD and DD laminates during 30 J LVI event.

Table 6
CAI responses of QUAD and DD laminates.

Compression after 75 J impact				
	QUAD	DD1	DD2	DD3
CAI residual strength (MPa)	267.5	272.6 (+1.9 %)	262.2 (−1.9 %)	279.4 (+4.4 %)
CAI effective modulus (GPa)	167.0	164.4 (−1.5 %)	187.3 (+12.1 %)	181.2 (+8.5 %)
Compression after 30 J impact				
	QUAD	DD1	DD2	DD3
CAI residual strength (MPa)	285.8	293.3 (+2.6 %)	284.7 (−0.4 %)	292.3 (+2.3 %)
CAI effective modulus (GPa)	167.2	165.8 (−0.9 %)	189.2 (13.1 %)	183.1 (+9.5 %)

4. Results and discussions

4.1. DD design range

When designing with QUAD laminates, the in-plane and flexural stiffnesses of the laminate can be tailored by changing the relative proportion and location of 0°, ±45°, and 90° plies in the laminate. The change of the stiffness can be demonstrated by plotting the geometry factors V^*_{A2} versus V^*_{A1} (or V^*_{D2} versus V^*_{D1} for the flexural stiffness). For example, by increasing the proportion of 0° plies in the QUAD laminate, both V^*_{A1} and V^*_{A2} increase, while increasing the proportion of 90° plies decreases V^*_{A1} and increases V^*_{A2}. On the other hand, increasing the proportion of ±45° plies would result in a lower V^*_{A2} with no effect on V^*_{A1}. Regarding the V^*_{D1} and V^*_{D2}, in addition to the percentage of 0°, 90°, and ±45° plies, the location of the plies with respect to the laminate's mid-plane is also an important factor.

The developed computer tool can plot V^*_{A2} versus V^*_{A1} and V^*_{D2} versus V^*_{D1} diagrams, hereafter called in-plane and flexural design range plots, respectively. The locations of the QUAD, DD1, DD2, and DD3 laminates in the in-plane and flexural design ranges are indicated in Fig. 5. The feasible design range with the DD concept is highlighted in both diagrams. In the in-plane design range, an equivalent DD does not exist for a QUAD laminate with more than 50 % of 0° or 90° plies. The upper boundaries of the in-plane design range are feasible when one of the DD angles is 90° (upper left boundary) or 0° (upper right boundary). In case the given QUAD is outside the DD design range boundaries, the developed computer tool can suggest a DD laminate with the closest possible [A*] or [D*] on the DD range boundaries. It should be noted that in the flexural design range, the location of the plies with respect to the laminate's mid-plane is also an important factor in determining whether the QUAD is in the DD design range. It is possible to have over 50 % of 0° or 90° plies but still be inside the DD flexural design range.

4.2. Impact simulation results

The impact damage areas after a 75 J impact event for the QUAD and DD laminates are compared in Fig. 6. In Fig. 6, the damage areas of each failure mode are superimposed and colored based on the ply numbers. The ply-by-ply damage areas are compared in Fig. 7. These areas were obtained by plotting the ply-by-ply failure modes and finding the area of a curve encompassing each failure mode in each ply. In all laminates, fiber kinking, and fiber splitting mostly occurred near the impacted face, where the compressive stress in the fiber direction was considerable. The matrix cracking area was larger in the plies near the back face and in the first two plies near the impacted face. The source of matrix cracking near the impacted face was high local shear stresses while the matrix cracking near the back face was induced by tensile stresses perpendicular to the fiber direction due to bending. In QUAD laminate, the superimposed matrix cracking and fiber splitting areas were slightly smaller, and the superimposed delamination area was larger compared to DD laminates. Comparing the DD laminates, the shapes of the damaged areas were different in each ply. Yet, there was no significant difference between the overall areas of each damage mode.

Overall, the trend of the matrix cracking, fiber splitting, and fiber kinking failure criteria was similar in QUAD and DD laminates, moving from the impacted face (Ply-1) to the back face (Ply-32). However, the delamination areas were different in QUAD compared with DD laminates. In QUAD laminate, the area of delamination near the mid-plane was larger than all DD laminates. This can be explained by higher interlaminar shear stresses in the QUAD laminate, which act as delamination driving forces. To this end, the interlaminar shear stresses were obtained for the QUAD and the three DD laminates using Yeoh et al. [43] analytical approach. Since the bending load is the main load in an

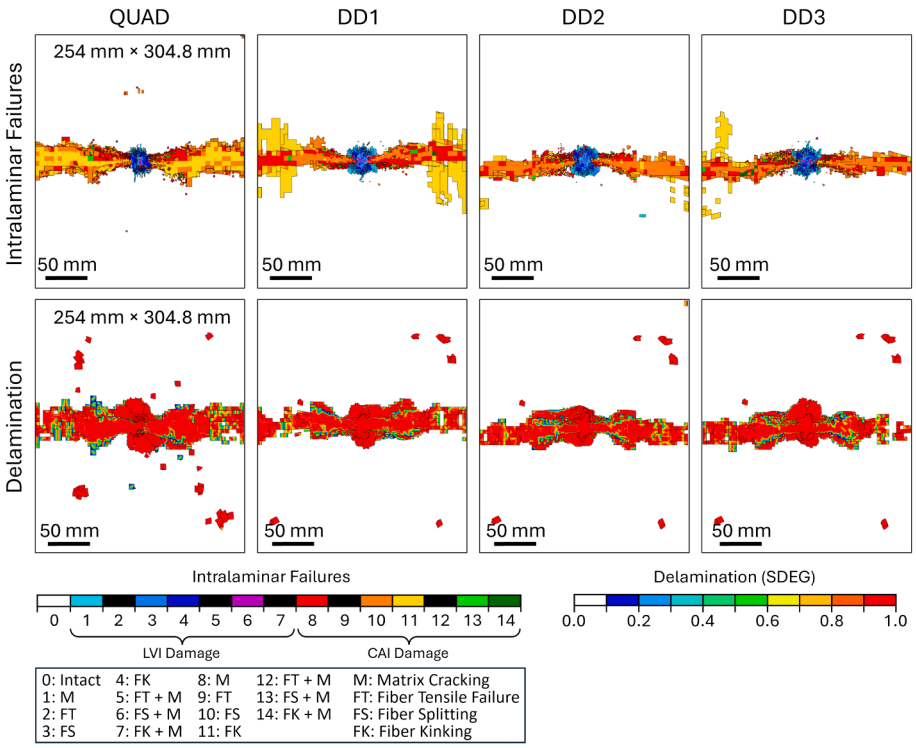

Fig. 11. Superimposed intralaminar failures and delamination areas for QUAD and DD laminates under compression after 75 J impact.

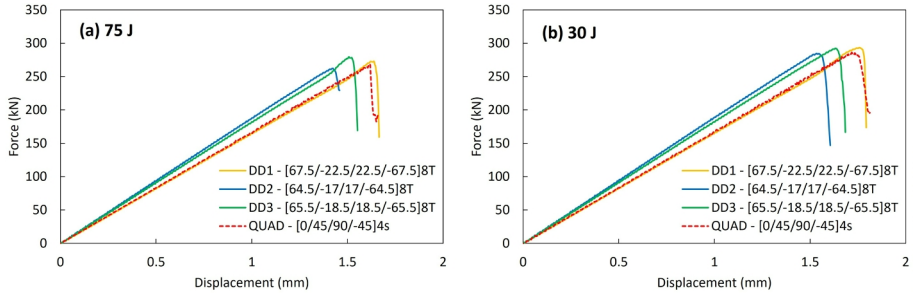

Fig. 12. CAI force–displacement diagrams for QUAD and DD laminates after 75 J and 30 J impact events.

impact event, the interlaminar shear stresses (τ_{xz} and τ_{yz}) were calculated under a bending loading condition, with a unit moment applied in the X and Y directions (X and Y are in-plane directions). The layer-by-layer interlaminar shear stress factors ($\tau_{xz}/\tau_{applied}$ and $\tau_{yz}/\tau_{applied}$) are plotted for QUAD and DD laminates in Fig. 8. The distribution of τ_{xz} in DD laminates was close to the parabolic distribution. This observation, which is common in homogeneous materials like metals, is attributed to the homogenized behavior of DD laminates. The differences in τ_{yz} stresses were the reason for the larger delamination areas in QUAD. In QUAD, near the mid-plane both τ_{xz} and τ_{yz} were high and their superposition was higher than that of DD laminates. It should be noted that in this analytical study, the variation in interlaminar shear strength and fracture toughness with the plies mismatch angle [44] have not been considered. Hence, to investigate the interlaminar failure in more detail in future studies, a more sophisticated analytical model accounting for the ratio of interlaminar shear stress to interlaminar strength is required.

The impact responses of the QUAD and the three DD laminates during the 75 J and 30 J impact events are compared in Fig. 9, Fig. 10 and Table 6. The difference in peak loads between the QUAD and the equivalent DD laminates was below 6.8 %, and the differences between the maximum displacement of the laminate's center and impact duration were less than 1.4 %. The impact response of DD2, which had a similar flexural stiffness [D*], was the most similar to that of the QUAD laminate.

4.3. CAI simulation results

The intralaminar failures and delamination areas after the CAI simulation are shown in Fig. 11 for the QUAD and the three DD laminates. The LVI and CAI intralaminar failure modes and their combinations are indicated with distinct colors. The failure modes indicated with black color did not occur during the impact scenario or the subsequent CAI simulation. In all laminates, the damage only occurred near the impacted region up to the final failure load. After reaching the failure load, all damage modes propagated from the impacted region to the lateral edges of the laminate. Overall, the damage areas of QUAD and DD laminates were similar. In DD1 and DD2 laminates, where the failure load was slightly higher, more fiber kinking was captured near the lateral edges after the failure occurrence. It should be noted that global buckling did not occur in any of the laminates.

The CAI force–displacement curves of QUAD and DD laminates after 75 J and 30 J impact events are compared in Fig. 12 and Table 6. Compared to the QUAD, DD1 and DD3 exhibited 1.9 % and 4.4 % higher CAI strengths after 75 J impact event, and 2.6 % and 2.3 % higher CAI

strengths after 30 J impact event, respectively. In contrast, DD2 showed 1.9 % and 0.4 % lower CAI strengths after 75 J and 30 J impact events. The effective modulus of the laminate under compression is mainly determined by the A_{11}^{*} component of the [A*] matrix. Therefore, the CAI characteristics of DD1, which had a similar in-plane stiffness [A*], were the most similar to that of the QUAD. The A_{11}^{*} in the DD2 and DD3 were 13.8 % and 9.6 % higher than that of QUAD.

5. Conclusions

The impact and CAI responses of a QUAD laminate ($[0/45/90/-45]_{4s}$) and three equivalent DD laminates were investigated using a validated high-fidelity FE model. Additionally, a computer tool was developed to assist in finding the equivalent DD and selecting the best stacking sequence in terms of meeting the homogenization criteria. Three DD layups were selected: DD1 ($[67.5/-22.5/22.5/-67.5]_{8T}$) had an equal in-plane stiffness [A*], DD2 ($[64.5/-17/17/-64.5]_{8T}$) had an equal flexural stiffness [D*], and DD3 ($[65.5/-18.5/18.5/-65.5]_{8T}$) had a similar [D*] matrix, while keeping the difference between each element of [A*] matrices below 10 %.

Overall, the DD1 laminate exhibited a similar behavior under CAI loading, DD2 showed a similar behavior under impact loading, and DD3's behavior was in between. Considering both overall impact damage areas and the CAI strengths, the conclusion can be drawn that QUAD laminates can be replaced by equivalent DD without compromising impact damage tolerance, while simultaneously providing the design and manufacturing ease benefits associated with the DD design. One limitation of using DD laminates is the minimum number of building block repetitions required to achieve a homogenized condition. This sets a limit for the minimum thickness of the laminate. Whereas replacing QUAD laminates with their DD equivalents shows potential as an innovative approach, further research is required to assess other aspects of DD laminates, such as the effect of ply dropping on the performance of components made with DD layup.

CRediT authorship contribution statement

Peyman Shabani: Writing – original draft, Visualization, Software, Methodology, Investigation, Data curation. **Lucy Li:** Writing – review & editing, Supervision, Funding acquisition, Conceptualization. **Jeremy Laliberte:** Writing – review & editing, Supervision, Funding acquisition, Conceptualization.

Declaration of competing interest

The authors declare that they have no known competing financial interests or personal relationships that could have appeared to influence the work reported in this paper.

Data availability

Data will be made available on request.

Acknowledgments

The authors would like to thank the Natural Sciences and Engineering Research Council (NSERC) and the Department of National Defence (DND) of Canada for the financial support provided for this research. This research was partly enabled by the computational support provided by the Digital Research Alliance of Canada (alliancecan.ca).

Appendix A. Supplementary data

Supplementary data to this article can be found online at https://doi.org/10.1016/j.compstruct.2024.118615.

References

[1] Tsai SW. Double–double: new family of composite laminates. AIAA J 2021;59:4293–305.
[2] Tsai SW, Melo JDD, Sihn S, Arteiro A, Rainsberger R. Composite Laminates: theory and practice of analysis, design and automated layup. Stanford Aeronaut. Astronaut. 2017.
[3] Kappel E. Unique manufacturing opportunity. DOUBLE-DOUBLE Simpl Des Manuf Compos Laminates 2023:71–94.
[4] Zhao K, Kennedy D, Miravete A, Tsai SW, Featherston CA, Liu X. Defining the design space for double-double laminates by considering homogenization criterion. AIAA J 2023;61:3190–203.
[5] Miravete A. Preferred stacking sequences for homogenization. DOUBLE-DOUBLE Simpl Des Manuf Compos Laminates 2023:95–136.
[6] Kappel E. Double-Double laminates for aerospace applications—finding best laminates for given load sets. Compos Part C Open Access 2022;8:100244.
[7] Shrivastava S, Sharma N, Tsai SW, Mohite PM. D and DD-drop layup optimization of aircraft wing panels under multi-load case design environment. Compos Struct 2020;248:112518.
[8] Vermes B, Tsai SW, Massard T, Springer GS, Czigany T. Design of laminates by a novel "double–double" layup. Thin-Walled Struct 2021;165:107954.
[9] Vermes B, Tsai SW, Riccio A, Di Caprio F, Roy S. Application of the Tsai's modulus and double-double concepts to the definition of a new affordable design approach for composite laminates. Compos Struct 2021;259:113246.
[10] Alves GC, Vignoli LL, Neto RMC. Damage onset in CFRP single lap joint for DD and QUAD laminates. J Mech Sci Technol 2024;38:157–62.
[11] Zhao M, Zhao Y, Wang A, Chang Z, Zhang J, Wang Z. Investigation of the mode-I delamination behavior of Double-Double laminate carbon fiber reinforced composite. Compos Sci Technol 2024;248:110463.
[12] Barbosa LG, Gomes GF. Numerical simulation of pressure vessel explosions using metallic and composite materials: a comparative study. Int J Hydrogen Energy 2024;58:289–301.
[13] Arteiro A. Notched response of DD laminates for robust characterization of design allowables. DOUBLE-DOUBLE Simpl Des Manuf Compos Laminates 2023:273–90.
[14] Liu JL, Yang G, Tay TE, Tan VBC, Jiang DZ, Zhi J. Uniaxial tensile strength of open-hole Double-Double laminates. DOUBLE-DOUBLE Simpl Des Manuf Compos Laminates 2023:291–302.
[15] Dantas da Cunha R, Targino TG, Cardoso C, da Costa P, Ferreira E, Freire Júnior RCS, et al. Low velocity impact response of non-traditional double-double laminates. J Compos Mater 2023;57:1807–17.
[16] Millen SLJ, Aravand MA, Ullah Z, Falzon B. Studies on the impact and compression-after-impact response of 'Double-Double'carbon-fibre reinforced composite laminates. DOUBLE-DOUBLE Simpl Des Manuf Compos Laminates 2023:161–80.
[17] Kappel E, Boose Y, Mißbach M. A CAI study on transition zones of conventional and Double-Double laminates. Compos Part C Open Access 2024;14:100450.
[18] Shabani P, Li L, Laliberte J, Qi G, Rapking D, Mollenhauer D. High-fidelity simulation of low-velocity impact damage in fiber-reinforced composite laminates using integrated discrete and continuum damage models. Compos Struct 2023;116910.
[19] Shabani P, Li L, Laliberte J, Qi G. Compression after impact (CAI) failure mechanisms and damage evolution in large composite laminates: High-fidelity simulation and experimental study. Compos Struct 2024:118143.
[20] Tsai SW, Hahn HT. Introduction to composite materials. Technomic Publishing Company; 1980.
[21] McQuien JS, Hoos KH, Ferguson LA, Iarve EV, Mollenhauer DH. Geometrically nonlinear regularized extended finite element analysis of compression after impact in composite laminates. Compos Part A Appl Sci Manuf 2020;134:105907.
[22] Shabani P, Taheri-Behrooz F, Samareh-Mousavi SS, Shokrieh MM. Very high cycle and gigacycle fatigue of fiber-reinforced composites: a review on experimental approaches and fatigue damage mechanisms. Prog Mater Sci 2021;118:100762.
[23] ASTM D7137/D7137M-17. Standard test method for compressive residual strength properties of damaged polymer matrix composite plates. ASTM Int 2017.
[24] Sachse R, Pickett AK, Middendorf P. Simulation of impact and residual strength of thick laminate composites. Compos Part B Eng 2020;195:108070.
[25] Lin S, Ranatunga V, Waas AM. Experimental study on the panel size effects of the Low-Velocity Impact (LVI) and Compression After Impact (CAI) of laminated composites, Part I: LVI. Compos Struct 2022;115822.
[26] Cheng Z-Q, Tan W, Xiong J-J. Modelling pre-fatigue, low-velocity impact and post-impact fatigue behaviours of composite helicopter tail structures under multipoint coordinated loading spectrum. Thin-Walled Struct 2022;176:109349.
[27] Cheng Z, Xiong J. Progressive damage behaviors of woven composite laminates subjected to LVI. TAI and CAI Chinese J Aeronaut 2020;33:2807–23.
[28] Cheng Z-Q, Tan W, Xiong J-J. Progressive damage modelling and fatigue life prediction of plain-weave composite laminates with low-velocity impact damage. Compos Struct 2021;273:114262.
[29] Kaddour A-S, Hinton MJ. Maturity of 3D failure criteria for fibre-reinforced composites: Comparison between theories and experiments: Part B of WWFE-II. J Compos Mater 2013;47:925–66.
[30] Shabani P, Li L, Laliberte J, Qi G. Low-velocity impact damage simulation using cohesive zone model and LaRC05 criterion with efficient search algorithm. 23rd Int Conf Compos Mater 2023.
[31] Shabani P, Li L, Laliberte J, Qi G. Enhanced LaRC05 failure criteria for investigating low-velocity impact on fiber-reinforced composites: an experimental and computational study. Aerosp Sci Technol 2024;109554.

[32] Martín-Santos E, Maimí P, González EV, Cruz P. A continuum constitutive model for the simulation of fabric-reinforced composites. Compos Struct 2014;111:122–9.
[33] Rivallant S, Bouvet C, Hongkarnjanakul N. Failure analysis of CFRP laminates subjected to compression after impact: FE simulation using discrete interface elements. Compos Part A Appl Sci Manuf 2013;55:83–93.
[34] Pinho ST, Darvizeh R, Robinson P, Schuecker C, Camanho pp.. Material and structural response of polymer-matrix fibre-reinforced composites. J Compos Mater 2012;46:2313–41.
[35] Hongkarnjanakul N, Bouvet C, Rivallant S. Validation of low velocity impact modelling on different stacking sequences of CFRP laminates and influence of fibre failure. Compos Struct 2013;106:549–59.
[36] Schirmaier FJ, Weiland J, Kärger L, Henning F. A new efficient and reliable algorithm to determine the fracture angle for Puck's 3D matrix failure criterion for UD composites. Compos Sci Technol 2014;100:19–25.
[37] Clay SB, Knoth PM. Experimental results of quasi-static testing for calibration and validation of composite progressive damage analysis methods. J Compos Mater 2017;51:1333–53.
[38] Yong M, Falzon BG, Iannucci L. On the application of genetic algorithms for optimising composites against impact loading. Int J Impact Eng 2008;35:1293–302.
[39] Maimí P, Camanho PP, Mayugo JA, Dávila CG. A continuum damage model for composite laminates: Part II–Computational implementation and validation. Mech Mater 2007;39:909–19.
[40] Nairn JA, Harper SI, Bascom WD. Effects of fiber, matrix, and interphase on carbon fiber composite compression strength. Contract Rep 1994;4601:NASA.
[41] Abdulhamid H, Bouvet C, Michel L, Aboissiere J, Minot C. Numerical simulation of impact and compression after impact of asymmetrically tapered laminated CFRP. Int J Impact Eng 2016;95:154–64.
[42] Camanho PP, Bessa MA, Catalanotti G, Vogler M, Rolfes R. Modeling the inelastic deformation and fracture of polymer composites–Part II: Smeared crack model. Mech Mater 2013;59:36–49.
[43] Yeoh KM, Liu JL, Tay TE, Tan VB. Interlaminar shear stress and failure of quad and double-double laminates. DOUBLE-DOUBLE Simpl Des Manuf Compos Laminates 2023:181–205.
[44] Kim BW, Mayer AH. Influence of fiber direction and mixed-mode ratio on delamination fracture toughness of carbon/epoxy laminates. Compos Sci Technol 2003;63:695–713.